



Dual response signal CdTe QDs@ZIF-8 with butterfly spectrum for dual-mode fluorescence/colorimetric detection of tetracycline in animal feeds

Yingfei Hui¹ · Mingyue Wang¹ · Yinsheng Liu¹ · Liping Peng¹ · Jiaying Tian¹ · Borong Ren¹ · Hao Guo¹ · Wu Yang¹

Received: 18 June 2024 / Revised: 3 August 2024 / Accepted: 19 August 2024
© The Author(s), under exclusive licence to Springer-Verlag GmbH, DE part of Springer Nature 2024

Abstract

In this study, a ratiometric fluorescent sensor CdTe QDs@ZIF-8 with butterfly spectra is successfully constructed by in situ encapsulating mercaptopropionic acid-modified CdTe quantum dots in zeolitic imidazolate framework-8 (ZIF-8) with a simple strategy, and used for the detection of tetracycline in fluorescence/smartphone colorimetry dual-mode. ZIF-8 not only reduces the agglomeration of the quantum dots but also surprisingly generates a new green fluorescence signal at 524 nm while the red fluorescence of the CdTe quantum dots at 650 nm quenches when tetracycline is added. The two opposing fluorescence signals create a butterfly-shaped fluorescence spectrum, allowing the sensor to detect tetracycline over a linear range of 0–70 μM with the detection limit (LOD) of 0.0155 μM by using a ratiometric fluorescence technique. What is more, based on the obvious color change of the fluorescent sensor gradually from red to green under UV light, a highly stable point-of-care testing sensor has been developed for on-site detection of tetracycline through color recognition by smartphones, which can be used for real-time detection of this antibiotic in the range of 0–1000 μM with the LOD of 0.0249 μM . This work provides a simple and efficient method for the on-site detection of tetracycline.

Keywords Metal–organic frameworks · Quantum dots · Tetracycline · Point-of-care test · Ratiometric fluorescent sensors · Visual inspection

Introduction

Tetracycline (TC) is a broad-spectrum antibiotic that is widely used as a growth promoter in animal feed, and therefore, it has a high probability of being present in food of animal origin [1–4]. In addition, TC can accumulate in the food chain through bioconcentration, but the digestive systems of humans and animals are unable to metabolize TC with complex molecular structures, which leads to water contamination and ecosystem balance disruption, and poses a serious threat to human health [5–8]. In the standard set by the Ministry of Agriculture of the People's Republic of China, the maximum residue limit (MRL) for tetracycline

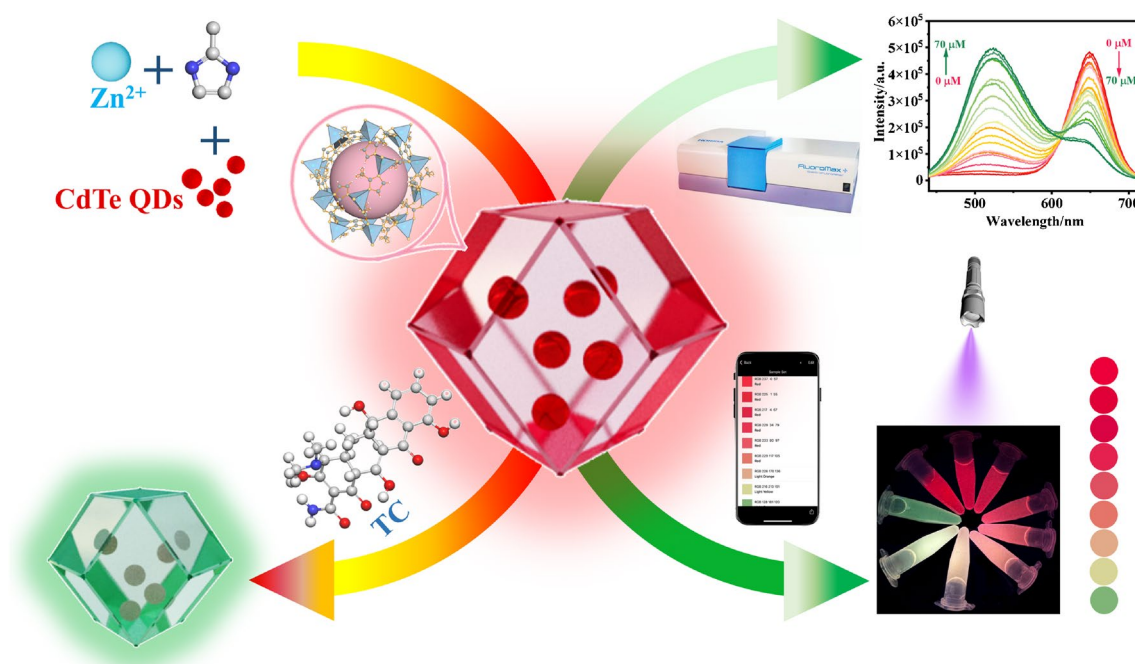
is 3384 ng L^{-1} in water and 200 $\mu\text{g kg}^{-1}$ in animal foods [9]. In the European Union, the addition of tetracycline to feed has been banned since 2017 and the MRL in food of animal origin is set at 100 $\mu\text{g kg}^{-1}$ [10, 11]. Therefore, the development of a highly sensitive and low-cost method for the detection of TC antibiotics is crucial.

Currently, the main methods for the detection of tetracycline are high-performance liquid chromatography [12, 13], colorimetric methods [14], and electrochemical analysis [15]. Although these methods are sensitive and accurate, they require complex sample pretreatment and time-consuming operation, which limits their application in the on-site detection of TC. In the rapidly evolving field of point-of-care testing (POCT), fluorescent assays offer the advantages of high sensitivity, real-time detection, low cost, and simplicity of operation to meet the need for rapid detection of TC in resource-limited settings [16–22]. Moreover, the construction of ratiometric fluorescence platforms with dual-emission properties can broaden the range of color variations, rather than just color brightness, for easier visual detection, which is important for the implementation of POCT [23–28].

✉ Hao Guo
haoguo12@126.com

✉ Wu Yang
xbsfda123@126.com

¹ College of Chemistry and Chemical Engineering, Northwest Normal University, Lanzhou 730070, Gansu, PR China



Scheme 1 Synthesis of CdTe QDs@ZIF-8 and fluorescence/smartphone colorimetric detection

In recent years, combining the unique photophysical properties of the aggregation-induced emission (AIE) structures into metal–organic frameworks (MOFs) systems has been considered as an available method to obtain fluorescent composites with enhanced AIE properties [29–35]. For example, Guo et al. encapsulated Au NCs in MOFs for the detection of mercury ions and captopril. The tethering effects of MOFs can restrict the motion of Au NCs, which triggers AIE effect, resulting in a significant enhancement of the fluorescence of Au NCs [36]. Zhu et al. developed a fluorescent enzyme-linked immunosorbent assay (FELISA) for bisphenol S in beverages by encapsulating copper nanoclusters (Cu NCs) with AIE property into ZIF-8. The integration of AIE building blocks into the porous ZIF-8 showed significant advantages in improving the analytical performance of FELISA [37]. However, few studies have been carried out to utilize the tethering effect of MOF to trigger the AIE effect for detection purpose.

Based on the above considerations, we in situ encapsulated mercaptopropionic acid-modified CdTe quantum dots in the zeolite imidazolium ester backbone ZIF-8 by a simple one-pot method as a core component for target recognition and signal transduction. Quantum dots (QDs) are a new type of nanomaterials, among which typical CdTe quantum dots (CdTe QDs) are characterized by stable optical properties, large Stokes shifts, tunable emission wavelengths, and narrow emission spectra [38–44]. By using the “Bottle around ship” strategy, ZIF-8 grows around CdTe QDs, which allows more quantum dots to be embedded in the MOF, prevents

the leakage of quantum dots, solves the problem of quantum dot agglomeration more effectively, and greatly improves the stability of the quantum dots [45]. When TC was added, a new green fluorescence at 524 nm was generated while the red fluorescence at 650 nm was quenched in the CdTe QDs@ZIF-8, resulting in a butterfly-shaped fluorescence emission, which led to a secondary amplification of the signal and achieved a more sensitive detection of tetracycline. The constructed ratiometric fluorescence sensor (I_{524}/I_{650}) had a built-in self-calibration function that avoids interferences from factors unrelated to the analysis, resulting in higher sensitivity and more visible visual detection during quantitative analysis. A continuous change in color from bright red to green was also observed, which was easy to be distinguished with the naked eye. As a result, a sensitive visual inspection platform in conjunction with a smartphone was designed. Overall, the strategy provides a robust solution for monitoring tetracycline with good stability, portability, and sensitivity (Scheme 1).

Experimental section

Materials

All chemicals used are analytical and without further purification. Tetracycline (TC), chlortetracycline (CTC), and oxytetracycline (OTC) were purchased from Shanghai Macklin Biochemical Technology Co., Ltd (China). Cadmium

chloride hydrate ($\text{CdCl}_2 \cdot 2.5\text{H}_2\text{O}$), $\text{Zn}(\text{NO}_3)_2 \cdot 6\text{H}_2\text{O}$, NaOH, sodium borohydride (NaBH_4), and tellurium powder were obtained from Shanghai Zhongqin Chemical Reagent Co., Ltd (China). The amino acids required including alanine (Ala, 98%, AR), tryptophan (Try, 98%, AR), isoleucine (Ile, 99%, AR), cysteine (Cys, 98%, AR), tyrosine (Tyr, 98%, AR), phenylalanine (Ph, 98%, AR), arginine (Arg, 98%, AR), methionine (Met, 99%, AR), and proline (Pro, 99%, AR) were purchased from Shanghai Aladdin Chemistry Co., Ltd (China). Methanol, 3-mercaptopropionic acid (MPA), anhydrous ethanol, and methanol were purchased from Chengdu Forest Science & Technology Development Co., Ltd (China). Animal feed was purchased from the local market.

Synthesis of CdTe QDs

CdTe QDs were synthesized by a slightly modified reference method [46]. Firstly, NaHTe was prepared. 0.0638 g of tellurium powder and 0.1 g of NaBH_4 were first added to a Shrek flask, and the reaction was carried out by adding 10 mL of distilled water under a nitrogen atmosphere in an ice bath followed by vigorous stirring for 8 h. The black powder gradually disappeared and the solution changed to lilac. 0.2284 g of $\text{CdCl}_2 \cdot 2.5\text{H}_2\text{O}$ and 210 μL MPA were mixed in a three-necked flask, and then, 125 mL of distilled water was added and pH was adjusted to 9 with 1 M NaOH. When NaHTe solution (the supernatant) was added under nitrogen atmosphere, the solution rapidly changed from colorless to orange. The mixture solution was stirred at room temperature for 20 min and then refluxed at 100 °C for 48 h to obtain red QDs.

Synthesis of CdTe QDs@ZIF-8

The composite was prepared by referring to the literature method [47]. Typically, 1.50 g of $\text{Zn}(\text{NO}_3)_2 \cdot 6\text{H}_2\text{O}$ was dissolved in 60 mL of methanol, and then, 10 mL of CdTe QDs was added and stirred well to obtain solution A. 3.30 g of 2-methylimidazole was dissolved in 60 mL of methanol to obtain solution B. The solution B was poured into solution A and stirred at room temperature for 4 h. The product was washed with methanol and dried in a vacuum oven at 50 °C overnight. The obtained product was named as CdTe QDs@ZIF-8. ZIF-8 was synthesized by the same procedure except without adding CdTe QDs.

Characterization

The materials were characterized by Fourier transform infrared (FTIR) spectroscopy using an FTS-3000 FTIR spectrometer (Digilab, USA). Powder X-ray diffraction (PXRD) patterns were obtained by a D8 Advance X-ray diffractometer

(BRUKER, Germany). The morphology was analyzed on a Zeiss ULTRRA Plus (DENKO, Japan) scanning electron microscope (SEM). Transmission electron microscopy (TEM) images were acquired on a transmission electron microscope (FEI TecnaiG2-F20, USA). Adsorption and desorption isotherms were measured by an Autosorb N_2 adsorption–desorption analysis system (Quantachrome, Autosorb 1, USA). The surface chemical composition of the materials was measured by X-ray photoelectron spectroscopy (XPS, ThermoFisher Scientific, USA). The UV–Vis spectra of the compounds were determined by a T6 New Century Spectrophotometer (Beijing, China) at 190–1100 nm.

Fluorescence experiments

The excitation and emission spectra of the materials were measured at room temperature using a fluorescence Max-4 spectrophotometer from HORIBA, USA. The excitation and emission slit widths were 3 nm (90° orientation detection). One milligram of CdTe QDs@ZIF-8 was dispersed in 5 mL of H_2O and fluorescence detection was performed for different concentrations of TC (0–70 μM). The fluorescence spectra of the samples were measured under excitation wavelength at 355 nm.

Real sample analysis

Two different feeds were weighed for 1 g each, and each sample was added 10 mL of ethanol and ultrasonically extracted and the supernatant was filtered for detection.

Results and discussion

Characterizations of ZIF-8 and CdTe QDs@ZIF-8

The phase compositions and crystallinity of ZIF-8 and CdTe QDs@ZIF-8 composites were analyzed by X-ray diffraction spectroscopy. As shown in Fig. 1a, the characteristic diffraction peaks of ZIF-8 are in good agreement with the simulation of ZIF-8 (CCDC: 823083) [48]. The positions and intensities of the diffraction peaks observed in CdTe QDs@ZIF-8 are consistent with those of the ZIF-8 diffraction peaks, which suggests that the introduction of the QDs does not affect the crystal configuration of ZIF-8. It is proved that ZIF-8 is a good carrier of QDs.

Formation of ZIF-8, CdTe QDs, and CdTe QDs@ZIF-8 was proved by IR spectroscopy (Fig. 1b). The peaks at 1563 and 1425 cm^{-1} in CdTe QDs spectrum were attributed to the stretching vibrations of C=O in the MPA [41]. In IR spectra of ZIF-8 and CdTe QDs@ZIF-8, the peak at 420 cm^{-1} was attributed to Zn–N stretching vibration; the peaks at 1306 cm^{-1} , 1144 cm^{-1} , and 994 cm^{-1} corresponded

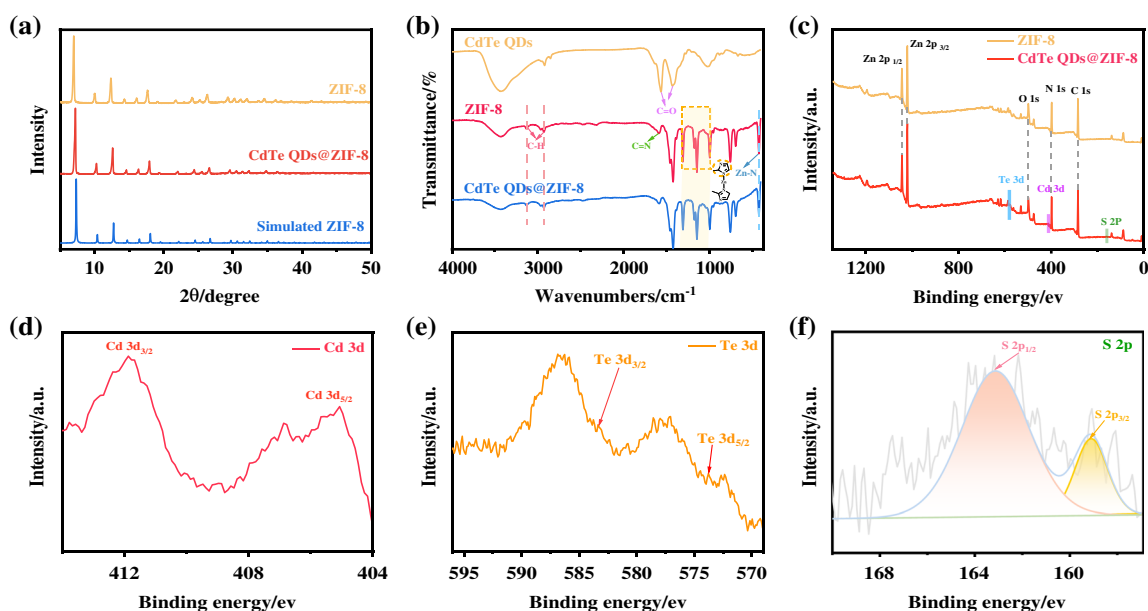


Fig. 1 **a** XRD patterns of the simulated ZIF-8 (blue line), experimental ZIF-8 (orange line), and CdTe QDs@ZIF-8 (red line). **b** FTIR spectra of CdTe QDs (orange line), ZIF-8 (red line), and CdTe QDs@

ZIF-8 (blue line). **c** XPS survey spectra of ZIF-8 (orange line) and CdTe QDs@ZIF-8 (red line). High-resolution XPS spectra of **(d)** Cd 3d, **(e)** Te 3d, and **(f)** S 2p in CdTe QDs@ZIF-8

to the in-plane bending vibration of the imidazole ring; and the peak at 1585 cm^{-1} was assigned to the $\text{C}=\text{N}$ stretching vibration while the bands located at 2928 cm^{-1} and 3134 cm^{-1} resulted from aromatic and aliphatic C-H stretching vibrations [33, 49]. The above results once again proved that quantum dots have been successfully introduced into ZIF-8 without changing the structure of the framework.

XPS analyses of ZIF-8 and CdTe QDs@ZIF-8 were carried out too. As shown in Fig. 1c, it could be seen that the prepared CdTe QDs@ZIF-8 not only contained the elements of zinc, carbon, nitrogen, and oxygen in ZIF-8 but also showed the presence of the elements of Cd, Te, and S [50]. In the Cd 3d spectrum (Fig. 1d), the double peaks centered at 411.9 and 405.1 eV were attributed to Cd $3d_{3/2}$ and Cd $3d_{5/2}$, respectively [51]. The Te 3d spectra (Fig. 1e) showed Te $3d_{3/2}$ and Te $3d_{5/2}$ spin-orbital doublets at 583.3 and 573.6 eV attributed to Te^{2-} , respectively, indicating formation of CdTe QDs. In addition, some peaks with higher binding energies were also observed, implying the presence of Te–O bond and the formation of tellurium oxide [50]. The Te 3d peak was found to be weak, probably due to the small amount of CdTe QDs encapsulated in ZIF-8. Additionally, approximately at 160 eV, a peak with doublet structure arising from S 2p was observed (Fig. 1f), corresponding to S $2p_{3/2}$ (159.1 eV) and S $2p_{1/2}$ (163.1 eV), respectively, which suggested the presence of Cd–SR bond [51]. These experimental results not only verified the successful synthesis of CdTe QDs but also further confirmed the formation of CdTe QDs@ZIF-8 composites.

The specific surface area and porosity of ZIF-8 and CdTe QDs@ZIF-8 were analyzed by N_2 adsorption–desorption isotherms (Figure S1). Both ZIF-8 and CdTe QDs@ZIF-8 exhibited typical type I isotherms, indicating that the structures were microporous [52]. After encapsulation of CdTe QDs, the specific surface area decreased from 1229.01 to $1133.85\text{ m}^2/\text{g}$, but the pore size did not change still at 10.01 \AA . This demonstrated that the ZIF-8 grew around the CdTe QDs.

The morphologies of ZIF-8 and CdTe QDs@ZIF-8 were characterized by SEM and TEM. Figure 2a–f show that ZIF-8 possessed a rhombic dodecahedron structure of approximately uniform size, and its structure did not change significantly after encapsulating CdTe QDs. From the TEM images of CdTe QDs, it could be seen that the average diameter of CdTe QDs was about 2.63 nm (Fig. 2g–i), which was larger than the average pore size of ZIF-8 ($\sim 1.01\text{ nm}$). Obviously, these quantum dots could not be directly inserted into pores of the MOFs, instead, the encapsulation was achieved by in situ growth of ZIF-8 around the CdTe QDs [45, 53]. On the other hand, the TEM image of CdTe QDs@ZIF-8 displayed lots of little black dots (CdTe QDs) in ZIF-8 matrix, which meant that the CdTe QDs had been successfully encapsulated in ZIF-8. Further evidence for the QDs encapsulation was also provided by EDX testing. The elemental mapping of CdTe QDs@ZIF-8 revealed that seven elements, namely, C, N, O, S, Zn, Te, and Cd, were uniformly distributed in the CdTe QDs@ZIF-8 (Fig. 2j). Simultaneously, the EDX spectrum of CdTe QDs@ZIF-8

Fig. 2 a–c SEM images of ZIF-8 at different magnifications. d–f SEM images of CdTe QDs@ZIF-8 at different magnifications. g–i TEM images of CdTe QDs at different magnifications. j–k TEM images of CdTe QDs@ZIF-8 at different magnifications. l EDX mapping of CdTe QDs@ZIF-8

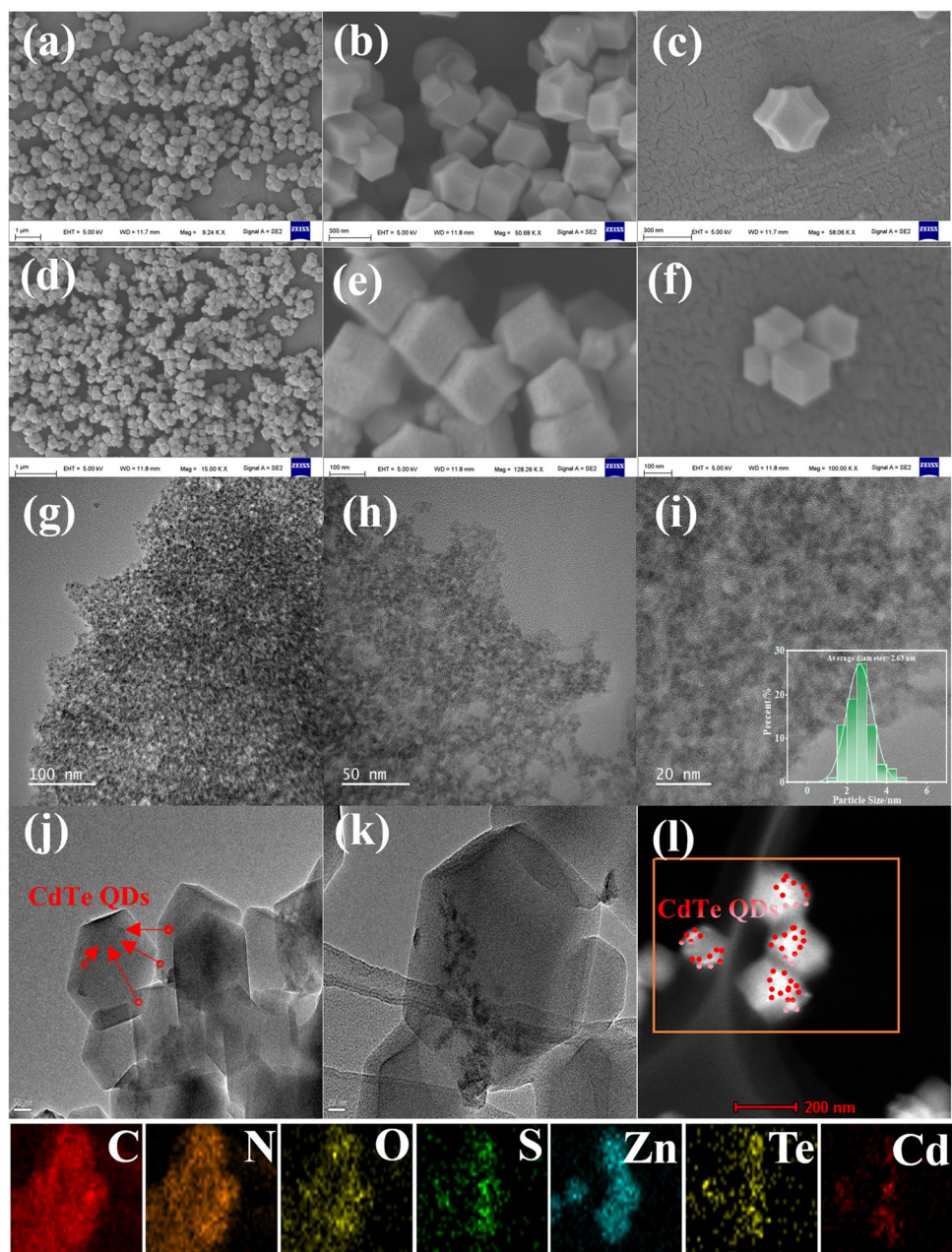


(Figure S2) also clearly showed coexistence of C, N, O, S, Zn, Te, and Cd elements (Cu element comes from the copper grid). The above results strongly confirmed the successful synthesis of CdTe QDs@ZIF-8.

Sensing performance of the ratiometric fluorescence sensor with butterfly spectra

Luminescence properties of ZIF-8 and CdTe QDs@ZIF-8 powders were compared under UV light and it was observed that ZIF-8 powder emitted blue fluorescence while CdTe QDs@ZIF-8 emitted red fluorescence (Figure S3). This proved the prepared composite

had excellent fluorescent property and also provided a possibility for the development of a fluorescent sensor. To assess the sensing performance of the prepared CdTe QDs@ZIF-8, its luminescence characteristics were investigated in detail at room temperature. Compared with CdTe QDs without ZIF-8 protection (Fig. 3a), it could be seen that the fluorescence of CdTe QDs was well preserved except for a slight redshift after they were encapsulated in ZIF-8. The redshift is mainly due to the specific interaction between CdTe QDs and ZIF-8 during the formation of the composite [24]. Figure 3b exhibits that the maximum excitation wavelength of CdTe QDs@ZIF-8 was 355 nm.

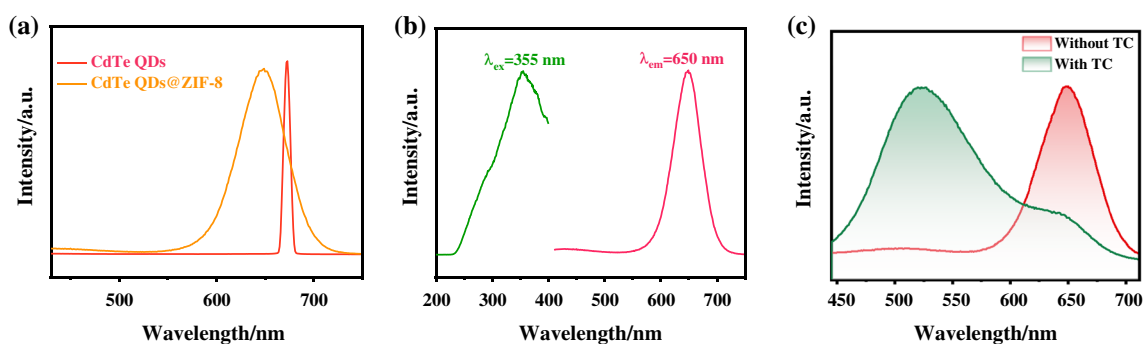


Fig. 3 **a** Fluorescence emission spectra of CdTe QDs (red line) and CdTe QDs@ZIF-8 (orange line). **b** Fluorescence excitation (green line) and emission (red line) spectra of CdTe QDs@ZIF-8. **c** Fluorescence emission spectra of CdTe QDs@ZIF-8 before (red line) and

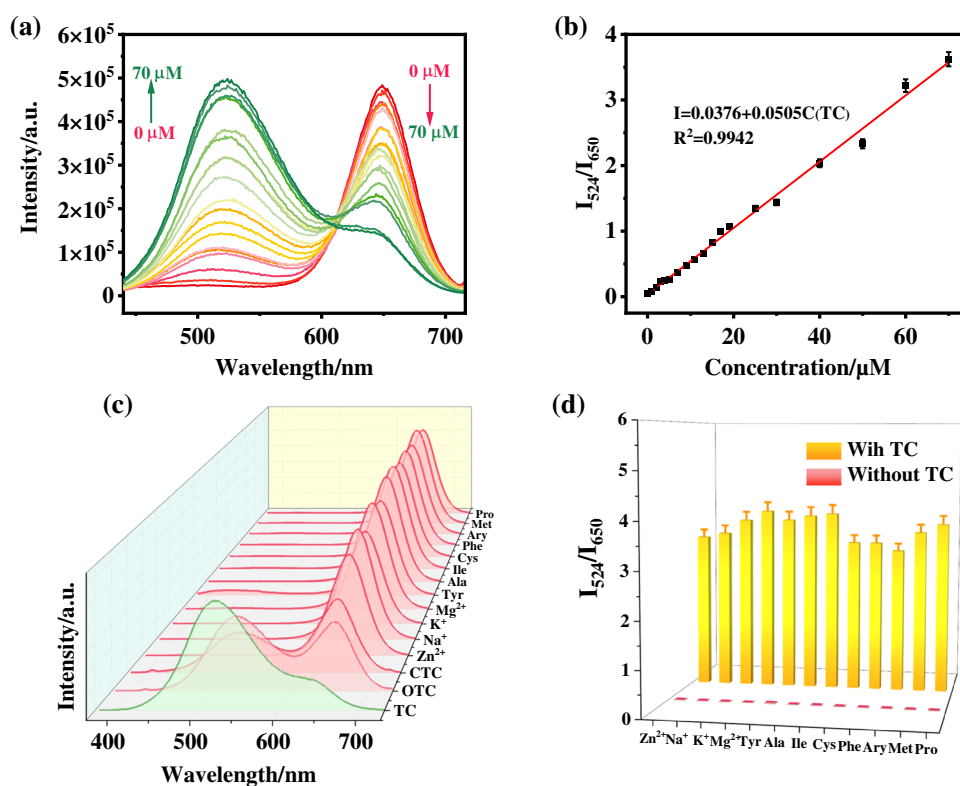
after (green line) TC addition

Figure 3c shows that when TC was added, a new fluorescence peak appeared at 524 nm whereas the fluorescence of CdTe QDs@ZIF-8 at 650 nm was significantly quenched at the same excitation wavelength. At the same time, the fluorescence intensity ratio I_{524}/I_{650} at 524 nm and 650 nm increased significantly with the increase of the TC concentration. This result indicated that CdTe QDs@ZIF-8 could be used as a ratiometric fluorescence sensor for quantitative analysis of TC.

Then, the response sensitivity of CdTe QDs@ZIF-8 to TC was explored. As shown in Fig. 4a, with TC concentration increasing, the fluorescence intensity at 524 nm

gradually enhanced whereas the fluorescence intensity at 650 nm accordingly decreased, so that the fluorescence emission spectrum showed a butterfly-shaped change. The CIE chromaticity diagram coordinates (Figure S4) were shifted from the original red region (0.3168, 0.5059) to the green region (0.5869, 0.3127). The linear relationship between the fluorescence intensity ratio I_{524}/I_{650} of CdTe QDs@ZIF-8 and TC concentration was tested under 355-nm excitation (Fig. 4b), and it was found that the ratio showed a good linear response with TC concentration in the range of 0–70 μM with a linear regression equation $I_{524}/I_{650} = 0.0376 + 0.0505C(\text{TC})$ ($R^2 = 0.9942$). The limit of

Fig. 4 **a** Fluorescence spectra of CdTe QDs@ZIF-8 with different concentrations of TC. **b** Linear relationship between the specific intensity (I_{524}/I_{650}) of CdTe QDs@ZIF-8 sensor and TC concentration. **c** Selectivity and **d** anti-interference test of CdTe QDs@ZIF-8 sensor against amino acids and metal cations



detection (LOD) was calculated to be $0.0155 \mu\text{M}$ according to the standard definition of IUPAC ($\text{LOD} = 3S_b/K$), where K is the slope of the fitted line and S_b is the standard deviation of 20 blank solutions. In addition, the method has a better linear range and wider detection limit compared to existing methods for the detection of TC (Table S1). As a result, the prepared CdTe QDs@ZIF-8 show high performance for TC detection.

As shown in Figure S5a, the TC-induced luminescence at 524 nm rapidly enhanced and simultaneously the luminescence at 650 nm rapidly decreased with the response time and the intensity ratio reached maximum and maintained stable after 7 min. The results indicated that the sensor possessed a rapid response toward TC detection, which can satisfy the requirement of rapid quantification of antibiotics in real samples. In addition, the sensor had excellent acid–base resistance and the intensity ratio almost kept unchanged in the pH 4–10 range (Figure S5b). The improved stability was attributed to the protection of the ZIF-8 shell against the aggregation and oxidation of CdTe QDs, which further confirmed the effectiveness of this ratiometric luminescence assay for the detection of TC in real samples.

Common interfering substances in animal feed and other kinds of tetracycline antibiotics were selected to further evaluate the selectivity of the sensor for TC detection. As shown in Fig. 4c, oxytetracycline (OTC) and chlorotetracycline (CTC) can trigger the response of the CdTe QDs@ZIF-8 sensor, but they were not as sensitive as TC, while the signals caused by other interfering molecules are almost negligible. Thus, it was demonstrated that the sensor had a satisfactory selectivity for TC detection. In addition, the anti-interference property of the sensor was further measured, and it can be seen that the fluorescence of CdTe QDs@ZIF-8 was hardly affected even though the concentration of interfering molecules was ten times that of TC (Fig. 4d). These results indicated that our material had an excellent anti-interference performance and can be used for the detection of TC in real samples.

Sensing mechanism of the ratiometric fluorescent sensor with butterfly spectra

As shown in Fig. 5a–d, the unique structure of tetracycline enables it to bind ZIF-8 specifically through

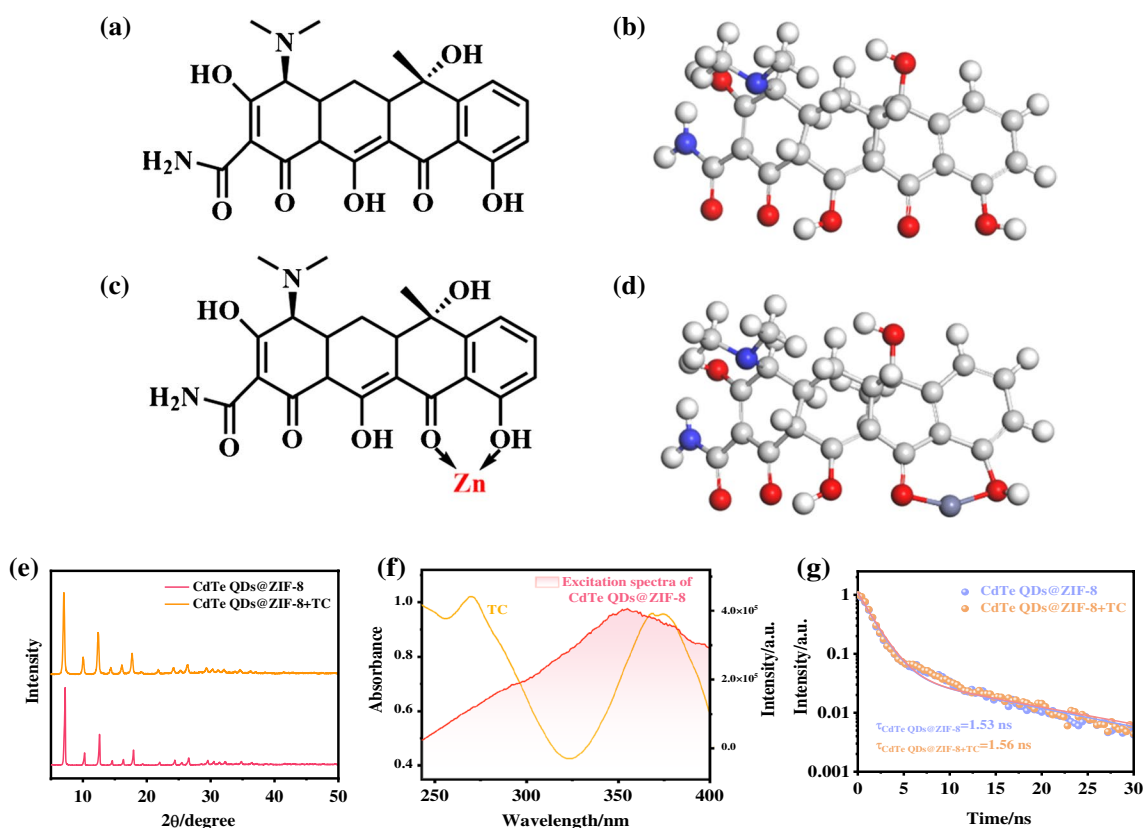


Fig. 5 Planar (a) and stereo (b) molecular structures of TC. Planar (c) and stereo (d) molecular structures of TC-Zn(II) compounds. **e** XRD patterns of CdTe QDs@ZIF-8 before (red line) and after (orange line) the addition of TC. **f** Overlapping of UV absorption spectra of tetra-

racycline (orange line) and fluorescence excitation spectra of CdTe QDs@ZIF-8. **g** Fluorescence decay curves of CdTe QDs@ZIF-8 and CdTe QDs@ZIF-8 + TC

hydrogen bonding, electrostatic, π - π stacking, and coordination interactions, which gives the ZIF composite good adsorption properties to strongly enrich tetracycline, triggering the aggregation-induced emission (AIE) effect leading to the formation of luminophores. At the same time, the interaction of TC with Zn^{2+} in QDs@ZIF-8 enlarges the rigid planar area and the conjugated π -system inside the TC.

To investigate the fluorescence quenching mechanism of CdTe QDs@ZIF-8 at 650 nm by TC, the XRD spectra of the samples before and after TC treatment were first compared and analyzed (Fig. 5e). The results showed that the XRD spectra of CdTe QDs@ZIF-8 did not change significantly after the addition of TC, which indicated that the material was not damaged. The UV absorption spectrum of TC was then tested. As seen from Fig. 5f, UV absorption spectrum of TC overlapped considerably with the fluorescence excitation spectrum of the composite, which triggered the inner filter effect (IFE), leading to the occurrence of fluorescence quenching. Next, the fluorescence lifetime of CdTe QDs@ZIF-8 was investigated in the presence and absence of TC. As seen in Fig. 5g, the fluorescence lifetime remained constant before and after TC addition, indicating that static quenching dominates the detection process. That is to say, fluorescence decay of the QDs is an IFE-caused static quenching process.

Detection of TC in real samples

The usefulness of the sensor in the analysis of real samples was verified by spiking recovery experiments in two different animal feeds (Table 1). The recoveries of TC ranged from 99.3 to 103.9% with RSDs of 1.12 to 3.28%. This indicated that the constructed CdTe QDs@ZIF-8 ratiometric fluorescence sensor has a strong potential for application in real samples.

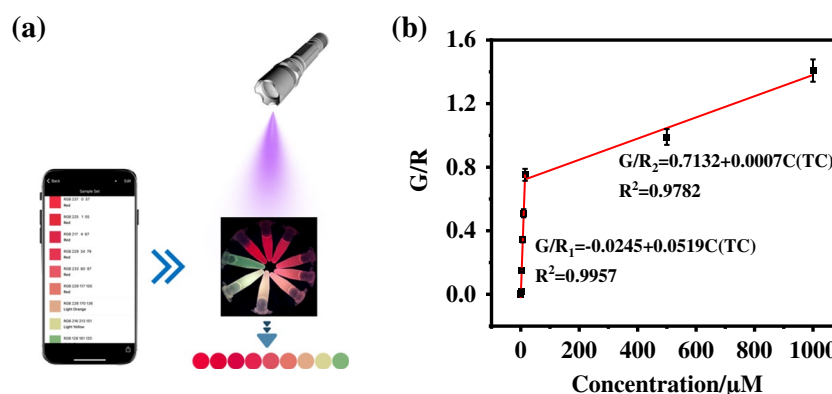
Visual detection of TC

A POCT platform for TC was developed by taking advantage of the excellent distinguishability and high stability of the ratiometric fluorescent sensor CdTe QDs@ZIF-8 (Fig. 6a). After the reaction of CdTe QDs@ZIF-8 with different concentrations of TC, a clear change in color from red, orange, and yellow gradually to green can be observed under UV light with 365-nm excitation. Photographs were taken by the smartphone iPhone 15 Pro and RGB values were extracted from the photograph using color scanning software. The ratio of the G value to the R -value (G/R) was used as the readout signal for TC detection. As seen from Fig. 6b, there were good linear relationships between G/R and TC concentration at both ends. In the low concentration range of 0~15 μ M, the linear fitting equation

Table 1 Detection of TC in real samples

Samples	Background (μ M)	Added (μ M)	Found (μ M)	Recovery (%)	RSD ($n=3$) (%)
Animal feed 1	0	10	10.26	102.5	3.28
	0	20	20.15	100.7	1.14
	0	40	39.73	99.3	3.31
Animal feed 2	0	10	10.30	102.9	1.12
	0	20	20.73	103.6	2.77
	0	40	41.59	103.9	3.05

Fig. 6 **a** Schematic diagram of the CdTe QDs@ZIF-8 fluorescent sensor with smartphone readout for POCT of TC. **b** The ratio of G to R -value (G/R) versus TC concentration



was $G/R_1 = -0.0245 + 0.0519C(\text{TC})$ ($R^2 = 0.9957$). In the range of 15 ~ 1000 μM , the linear fitting equation was $G/R_2 = 0.7132 + 0.0007C(\text{TC})$ ($R^2 = 0.9782$). The LOD was calculated as 0.0249 μM based on $3S_0/K$. The results showed that the ratiometric fluorescence sensor could be used for the visual detection of TC.

Conclusion

In summary, a composite material CdTe QDs@ZIF-8 was successfully prepared by a facile method, which can be used for dual-mode detection of tetracycline by fluorescence/smartphone colorimetry. TC was combined with ZIF-8 based on its strong adsorption ability to produce strong green fluorescence. Simultaneously, the red fluorescence of the CdTe QDs was strongly quenched by TC-triggered inner filter effect. These results led to a butterfly-shaped emission spectrum and resulting secondary signal amplification, which achieved a sensitive ratiometric fluorescence detection of tetracycline. Meanwhile, based on the obvious color change from red to green, a visual TC detection platform was successfully developed with satisfactory results. The constructed sensor had good practicality and great potential in food safety and environmental monitoring.

Supplementary Information The online version contains supplementary material available at <https://doi.org/10.1007/s00216-024-05511-6>.

Acknowledgements The authors are very grateful to the National Natural Science Foundation of China (22364020), Natural Science Foundation of Gansu Province (20JR10RA083), Project of Gansu Excellent Doctoral (22JR5RA140), Key Lab of Bioelectrochemistry and Environmental Analysis of Gansu Province and Northwest Normal University Young Teachers Research Capacity Promotion Plan (NWNULKQN-18-23), and the Key Lab of Eco-Environments Related Polymer Materials of MOE.

Author contribution Yingfei Hui: writing—original draft, review, and editing. Mingyue Wang: visualization. Yinsheng Liu: formal analysis. Liping Peng: supervision. Jiaying Tian: project administration. Borong Ren: investigation. Hao Guo: funding acquisition. Wu Yang: conceptualization, supervision, funding acquisition, and writing—review and editing.

Declarations

Conflict of interest The authors declare no competing interests.

References

- Chen F, Ma J, Zhu Y, Li X, Yu H, Sun Y. Biodegradation performance and anti-fouling mechanism of an ICME/electro-biocarriers-MBR system in livestock wastewater (antibiotic-containing) treatment. *J Hazard Mater.* 2022;426:128064. <https://doi.org/10.1016/j.jhazmat.2021.128064>.
- Ghimpețeanu OM, Pogurschi EN, Popa DC, Dragomir N, Drăgoțoiu T, Mihai OD, Petcu CD. Antibiotic use in livestock and residues in food—a public health threat: a review. *Foods.* 2022;11(10):1430. <https://doi.org/10.3390/foods11101430>.
- Granados-Chinchilla F, Rodríguez C. Tetracyclines in food and feedingstuffs: from regulation to analytical methods, bacterial resistance, and environmental and health implications. *J Anal Methods Chem.* 2017;2017(1):1315497. <https://doi.org/10.1155/2017/1315497>.
- Liu Y, Wu Y, Wang L, Zhu L, Dong Y, Xu W. A ratiometric dual-fluorescent paper-based synthetic biosensor for visual detection of tetracycline on-site. *J Hazard Mater.* 2024;467:133647. <https://doi.org/10.1016/j.jhazmat.2024.133647>.
- Deng Y, Xiao T, She A, Li X, Chen W, Ao T, Ni F. One-step synthesis of iron and nitrogen co-doped porous biochar for efficient removal of tetracycline from water: adsorption performance and fixed-bed column. *J Environ Manage.* 2024;352:119984. <https://doi.org/10.1016/j.jenvman.2023.119984>.
- Kaur S, Pal B. Superior visible-light absorbing Ag@ZnO nanorods hybrid photocatalyst for efficient decomposition of commercial pharmaceuticals tetracycline and amoxicillin. *J Water Process Eng.* 2024;58:104765. <https://doi.org/10.1016/j.jwpe.2023.104765>.
- Liu Y, Guo H, Wu N, Peng L, Wang M, Tian J, Xu J, Yang W. Eu³⁺-functionalized nanoporous covalent organic frameworks for fluorescence detection and removal of tetracycline. *ACS Appl Nano Mater.* 2023;6(8):6627–36. <https://doi.org/10.1021/acsanm.3c00323>.
- Rameshwar SS, Sivaprakash B, Rajamohan N, Mohamed BA, Vo D-VN. Remediation of tetracycline pollution using MXene and nano-zero-valent iron materials: a review. *Environ Chem Lett.* 2023;21(5):2995–3022. <https://doi.org/10.1007/s10311-023-01623-0>.
- She WZ, Li CH, Li RS, Ling J, Cao Q. Construction of two-dimensional fluorescent covalent organic framework nanospheres for the detection and removal of tetracycline. *Sep Purif Technol.* 2024;330:125294. <https://doi.org/10.1016/j.seppur.2023.125294>.
- Moreno-González D, García-Campaña AM. Salting-out assisted liquid–liquid extraction coupled to ultra-high performance liquid chromatography–tandem mass spectrometry for the determination of tetracycline residues in infant foods. *Food Chem.* 2017;221:1763–9. <https://doi.org/10.1016/j.foodchem.2016.10.107>.
- Phiroonsoontorn N, Sansuk S, Santaladchaiyakit Y, Srijaranai S. The use of dissolvable layered double hydroxide components in an in situ solid-phase extraction for chromatographic determination of tetracyclines in water and milk samples. *J Chromatogr A.* 2017;1519:38–44. <https://doi.org/10.1016/j.chroma.2017.09.005>.
- Yang X, Zhang S, Yu W, Liu Z, Lei L, Li N, Zhang H, Yu Y. Ionic liquid-anionic surfactant based aqueous two-phase extraction for determination of antibiotics in honey by high-performance liquid chromatography. *Talanta.* 2014;124:1–6. <https://doi.org/10.1016/j.talanta.2014.02.039>.
- Zhang Z, Li X, Ding S, Jiang H, Shen J, Xia X. Multiresidue analysis of sulfonamides, quinolones, and tetracyclines in animal tissues by ultra-high performance liquid chromatography–tandem mass spectrometry. *Food Chem.* 2016;204:252–62. <https://doi.org/10.1016/j.foodchem.2016.02.142>.
- Liu B, Zhu H, Feng R, Wang M, Hu P, Pan J, Niu X. Facile molecular imprinting on magnetic nanozyme surface for highly selective colorimetric detection of tetracycline. *Sensor Actuat B-Chem.* 2022;370:132451. <https://doi.org/10.1016/j.snb.2022.132451>.
- Hosu O, Melinte G, Ștefan G, Casian M, Cristea C. Towards selective tetracycline recognition in wastewater based on gold nanovoids@aptamer sensing. *Electrochim Acta.* 2023;460:142556. <https://doi.org/10.1016/j.electacta.2023.142556>.
- Chen L, Li Z, Dou Y, Wang H, Chen C, Wang X. Ratiometric fluoroprobe based on Eu-MOF@Tb³⁺ for detecting tetracycline

- hydrochloride in freshwater fish and its application in rapid visual detection. *J Hazard Mater.* 2024;469:134045. <https://doi.org/10.1016/j.jhazmat.2024.134045>.
17. Liu Y, Li R, Liang F, Deng C, Seidi F, Xiao H. Fluorescent paper-based analytical devices for ultra-sensitive dual-type RNA detections and accurate gastric cancer screening. *Biosens Bioelectron.* 2022;197:113781. <https://doi.org/10.1016/j.bios.2021.113781>.
 18. Semeniak D, Cruz DF, Chilkoti A, Mikkelsen MH. Plasmonic fluorescence enhancement in diagnostics for clinical tests at point-of-care: a review of recent technologies. *Adv Mater.* 2023;35(34):2107986. <https://doi.org/10.1002/adma.202107986>.
 19. Wang H, Wang Y, Wang W, Zhang Y, Yuan Q, Tan J. Materials-functionalized point-of-care testing devices for pathogen detection. *Acc Mater Res.* 2023;4(12):1083–94. <https://doi.org/10.1021/accountsmr.3c00151>.
 20. Wang K, Meng X, Yan X, Fan K. Nanozyme-based point-of-care testing: Revolutionizing environmental pollutant detection with high efficiency and low cost. *Nano Today.* 2024;54:102145. <https://doi.org/10.1016/j.nantod.2023.102145>.
 21. Wu H, Fang Y, Tian L, Liu X, Zhou X, Chen X, Gao H, Qin H, Liu Y. AIE nanozyme-based long persistent chemiluminescence and fluorescence for POCT of pathogenic bacteria. *ACS Sens.* 2023;8(8):3205–14. <https://doi.org/10.1021/acssensors.3c00918>.
 22. Zhao L, Li L, Zhao Y, Zhu C, Yang R, Fang M, Luan Y. Aptamer-based point-of-care-testing for small molecule targets: from aptamers to aptasensors, devices and applications. *TrAC-Trend Anal Chem.* 2023;169:117408. <https://doi.org/10.1016/j.trac.2023.117408>.
 23. Chang H, Tan P, Chen X, Liu T, Lu Z, Sun M, Su G, Wang Y, Zou Y, Rao H, Wu C. Real-time intelligent detection of ethephon based on a high-throughput ratiometric fluorescent probe. *J Hazard Mater.* 2024;465:133156. <https://doi.org/10.1016/j.jhazmat.2023.133156>.
 24. Chi J, Song Y, Feng L. A ratiometric fluorescent paper sensor based on dye-embedded MOF for high-sensitive detection of arginine. *Biosens Bioelectron.* 2023;241:115666. <https://doi.org/10.1016/j.bios.2023.115666>.
 25. Dai Y, Xu W, Hong J, Zheng Y, Fan H, Zhang J, Fei J, Zhu W, Hong J. A molecularly imprinted ratiometric fluorescence sensor based on blue/red carbon quantum dots for the visual determination of thiamethoxam. *Biosens Bioelectron.* 2023;238:115559. <https://doi.org/10.1016/j.bios.2023.115559>.
 26. Liu Y, Wang M, Hui Y, Sun L, Hao Y, Ren H, Guo H, Yang W. Polyarylether-based COFs coordinated by Tb³⁺ for the fluorescent detection of anthrax-biomarker dipicolinic acid. *J Mater Chem B.* 2024;12(2):466–74. <https://doi.org/10.1039/D3TB02070C>.
 27. Shen Y, Wei Y, Gao X, Nie C, Wang J, Wu Y. Engineering an enzymatic cascade catalytic smartphone-based sensor for on site visual ratiometric fluorescence–colorimetric dual-mode detection of methyl mercaptan. *Environ Sci Technol.* 2023;57(4):1680–91. <https://doi.org/10.1021/acs.est.2c07899>.
 28. Wang D, Yu L, Li X, Lu Y, Niu C, Fan P, Zhu H, Chen B, Wang S. Intelligent quantitative recognition of sulfide using machine learning-based ratiometric fluorescence probe of metal-organic framework UiO-66-NH₂/PpIX. *J Hazard Mater.* 2024;464:132950. <https://doi.org/10.1016/j.jhazmat.2023.132950>.
 29. Cai Y, Zhu H, Zhou W, Qiu Z, Chen C, Qileng A, Li K, Liu Y. Capsulation of AuNCs with AIE effect into metal–organic framework for the marriage of a fluorescence and colorimetric biosensor to detect organophosphorus pesticides. *Anal Chem.* 2021;93(19):7275–82. <https://doi.org/10.1021/acs.analchem.1c00616>.
 30. Peng Y, Lei Y, Luo J, Hu X, Sun F, Yang Y, Guo M, Cai T. The inherent AIE feature revealed the drug molecular state in cyclodextrin metal–organic framework for enhanced stability and absorption. *Chem Eng J.* 2024;479:147654. <https://doi.org/10.1016/j.cej.2023.147654>.
 31. Rouhani F, Morsali A, Retailleau P. Simple one-pot preparation of a rapid response AIE fluorescent metal–organic framework. *ACS Appl Mater Interfaces.* 2018;10(42):36259–66. <https://doi.org/10.1021/acsami.8b12404>.
 32. Xie S, Liu Q, Zhu F, Chen M, Wang L, Xiong Y, Zhu Y, Zheng Y, Chen X. AIE-active metal–organic frameworks: facile preparation, tunable light emission, ultrasensitive sensing of copper(II) and visual fluorescence detection of glucose. *J Mater Chem C.* 2020;8(30):10408–15. <https://doi.org/10.1039/D0TC00106F>.
 33. Yang Y, Zhou Z, Wang T, Tian D, Ren S, Gao Z. MOF-on-MOF heterostructure boosting AIE sensing and triggered structural collapse for histamine detection. *Talanta.* 2024;270:125632. <https://doi.org/10.1016/j.talanta.2024.125632>.
 34. Yu L, Chen H, Yue J, Chen X, Sun M, Tan H, Asiri AM, Alamry KA, Wang X, Wang S. Metal–organic framework enhances aggregation-induced fluorescence of chlortetracycline and the application for detection. *Anal Chem.* 2019;91(9):5913–21. <https://doi.org/10.1021/acs.analchem.9b00319>.
 35. Zhang Y, Xiong T, Möslein AF, Mollick S, Kachwal V, Babal AS, Amin N, Tan JC. Nanoconfinement of tetraphenylethylene in zeolitic metal-organic framework for turn-on mechanofluorochromic stress sensing. *Appl Mater Today.* 2022;27:101434. <https://doi.org/10.1016/j.apmt.2022.101434>.
 36. Guo Y, Zhang J, Liu J, Wang N, Su X. A highly sensitive fluorescence “on–off–on” sensing platform for captopril detection based on AuNCs@ZIF-8 nanocomposite. *Anal Chim Acta.* 2023;1276:341649. <https://doi.org/10.1016/j.aca.2023.341649>.
 37. Zhu N, Yuan K, Xiong D, Ai F, Zeng K, Zhao B, Zhang Z, Zhao H. A high-throughput fluorescence immunoassay based on conformational locking strategy of MOFs to enhance AIE effect of CuNCs-CS for bisphenol S analysis in food samples. *Chem Eng J.* 2023;462:142129. <https://doi.org/10.1016/j.cej.2023.142129>.
 38. Chen ZJ, Huang AJ, Luo L, Xu ZL, Wang H. Simple dual-read-out immunosensor based on phosphate-triggered and potassium permanganate for visual detection of fenitrothion. *Biosens Bioelectron.* 2024;246:115872. <https://doi.org/10.1016/j.bios.2023.115872>.
 39. Ding C, Huang Y, Shen Z, Chen X. Synthesis and bioapplications of Ag₂S quantum dots with near-infrared fluorescence. *Adv Mater.* 2021;33(32):2007768. <https://doi.org/10.1002/adma.202007768>.
 40. Fu J, Zhou S, Zhao P, Wu X, Tang S, Chen S, Yang Z, Zhang Z. A dual-response ratiometric fluorescence imprinted sensor based on metal-organic frameworks for ultrasensitive visual detection of 4-nitrophenol in environments. *Biosens Bioelectron.* 2022;198:113848. <https://doi.org/10.1016/j.bios.2021.113848>.
 41. Gan Z, Zhang T, Hu Y, Zhen S, Hu X. A simple fluorescence-scattering ratiometric sensor for biothiols based on CdTe quantum dots. *Sensor Actuat B-Chem.* 2023;378:133168. <https://doi.org/10.1016/j.snb.2022.133168>.
 42. Liang N, Hu X, Li W, Wang Y, Guo Z, Huang X, Li Z, Zhang X, Zhang J, Xiao J, Zou X, Shi J. A dual-signal fluorescent sensor based on MoS₂ and CdTe quantum dots for tetracycline detection in milk. *Food Chem.* 2022;378:132076. <https://doi.org/10.1016/j.foodchem.2022.132076>.
 43. Yuan L, Yan M, Tao X, Yang X, Long W, Xia W, Liao H, Gong Y, Zhang K, Xia Z, Fu Q. Efficient synthesis of high-purity carbon dots via self-polymerization driven bottom-up growth for high-selectivity sensing and high-efficiency separation. *Carbon.* 2024;226:119169. <https://doi.org/10.1016/j.carbon.2024.119169>.
 44. Zhang R, Zhang L, Yu R, Wang C. Rapid and sensitive detection of methyl parathion in rice based on carbon quantum dots nano-fluorescence probe and inner filter effect. *Food Chem.* 2023;413:135679. <https://doi.org/10.1016/j.foodchem.2023.135679>.
 45. Aguilera-Sigalat J, Bradshaw D. Synthesis and applications of metal-organic framework–quantum dot (QD@MOF) composites.

- Coord Chem Rev. 2016;307:267–91. <https://doi.org/10.1016/j.ccr.2015.08.004>.
46. Zhang K, Zhou H, Mei Q, Wang S, Guan G, Liu R, Zhang J, Zhang Z. Instant visual detection of trinitrotoluene particulates on various surfaces by ratiometric fluorescence of dual-emission quantum dots hybrid. *J Am Chem Soc*. 2011;133(22):8424–7. <https://doi.org/10.1021/ja2015873>.
 47. Li N, Zhou L, Jin X, Owens G, Chen Z. Simultaneous removal of tetracycline and oxytetracycline antibiotics from wastewater using a ZIF-8 metal organic-framework. *J Hazard Mater*. 2019;366:563–72. <https://doi.org/10.1016/j.jhazmat.2018.12.047>.
 48. Yi K, Zhang L. Embedding dual fluoroprobe in metal-organic frameworks for continuous visual recognition of Pb^{2+} and PO_4^{3-} via fluorescence 'turn-off-on' response: agar test paper and fingerprint. *J Hazard Mater*. 2020;389:122141. <https://doi.org/10.1016/j.jhazmat.2020.122141>.
 49. Si Y, Li Y, Yang G, Zhang S, Yang L, Dai W, Wang H. Zeolitic imidazolate framework-8 for ratiometric fluorescence sensing tetracyclines in environmental water based on AIE effects. *Anal Chim Acta*. 2022;1199:339576. <https://doi.org/10.1016/j.aca.2022.339576>.
 50. Li YS, Jiang FL, Xiao Q, Li R, Li K, Zhang MF, Zhang AQ, Sun SF, Liu Y. Enhanced photocatalytic activities of TiO_2 nanocomposites doped with water-soluble mercapto-capped CdTe quantum dots. *Appl Catal B-Environ*. 2010;101(1):118–29. <https://doi.org/10.1016/j.apcatb.2010.09.016>.
 51. Li ZJ, Fan XB, Li XB, Li JX, Ye C, Wang JJ, Yu S, Li CB, Gao YJ, Meng QY, Tung CH, Wu LZ. Visible light catalysis-assisted assembly of Ni_n -QD hollow nanospheres in situ via hydrogen bubbles. *J Am Chem Soc*. 2014;136(23):8261–8. <https://doi.org/10.1021/ja5047236>.
 52. Wang Y, Wang B, Shi H, Zhang C, Tao C, Li J. Carbon nanodots in ZIF-8: synthesis, tunable luminescence and temperature sensing. *Inorg Chem Front*. 2018;5(11):2739–45. <https://doi.org/10.1039/C8QI00637G>.
 53. Tran A, Valleix R, Réveret F, Frezet L, Cisnetti F, Boyer D. Encapsulation of InP/ZnS quantum dots into MOF-5 matrices for solid-state luminescence: ship in the bottle and bottle around the ship methodologies. *Materials*. 2024;17(13):3155. <https://doi.org/10.3390/ma17133155>.

Publisher's Note Springer Nature remains neutral with regard to jurisdictional claims in published maps and institutional affiliations.

Springer Nature or its licensor (e.g. a society or other partner) holds exclusive rights to this article under a publishing agreement with the author(s) or other rightsholder(s); author self-archiving of the accepted manuscript version of this article is solely governed by the terms of such publishing agreement and applicable law.